

Non-Newtonian effects on the slip and mobility of a self-propelling active particle

Akash Choudhary¹, T. Renganathan¹ and S. Pushpavanam¹†

¹Department of Chemical Engineering, Indian Institute of Technology, Chennai,
TN 600036, India

(Received xx; revised xx; accepted xx)

Janus particles propel themselves by generating concentration gradients along their active surface. This generates a flow near the surface, known as the diffusio-osmotic slip, which propels the particle even in the absence of externally applied concentration gradients. In this work, we study the influence of viscoelasticity and shear-thinning/thickening (described by the second-order-fluid and Carreau model, respectively) on the slip of a Janus particle. Using matched asymptotic expansions, we provide an analytical expression for the modification of slip induced by the non-Newtonian behavior. Using the reciprocal theorem, we estimate the influence of this modification on the particle mobility. The current study also has implications on the understanding of the transport of complex fluids in diffusio-osmotic pumps.

1. Introduction

Synthetic active particles are micron and submicron sized colloidal particles which can propel themselves along predictable trajectories. The mechanism of self-propulsion occurs via generation of local concentration gradient at the surface, which arises due to variation in surface activity such as adsorption or reaction (Anderson 1989; Golestanian *et al.* 2005, 2007; Sharifi-Mood *et al.* 2013). These gradients create a tangential diffusio-osmotic flow in a region very near the surface, resulting in a force-free swimming motion (Brady 2011). These active particles play an important role in biomedical and industrial research. It offers potential applications in drug-delivery micromachines and controlled studies of microbial infections (Gao & Wang 2014). Furthermore, a suspension of active particles represents a non-equilibrium system which exhibits characteristics such as enhanced fluid mixing in complex fluids (Gomez-Solano *et al.* 2016) and inertia-less turbulence, which are also observed in microbial suspensions and granular matter (Patteson *et al.* 2016). Therefore, understanding such novel self-propelled systems provides insights which extend to a wide range of physical phenomena, making it intriguing from a scientific standpoint.

Several studies have focused on understanding and modeling the surface slip, swimming and self-assembly of active particles (Anderson 1989; Golestanian *et al.* 2007; Michelin & Lauga 2014; Rallabandi *et al.* 2019). However, most of these assume the surrounding medium to be a Newtonian fluid. Since a majority of potential applications of the synthesized active particles lie in drug-delivery and other areas of biological research (Patteson *et al.* 2016), understanding the influence of rheology is essential. Recently, Datt *et al.* (2015, 2017); Pietrzyk *et al.* (2019) and Natale *et al.* (2017) have studied the swimming of an axisymmetric active particle suspended in a non-Newtonian medium through an asymptotic approach based on the reciprocal theorem. These studies used

† Email address for correspondence: spush@iitm.ac.in

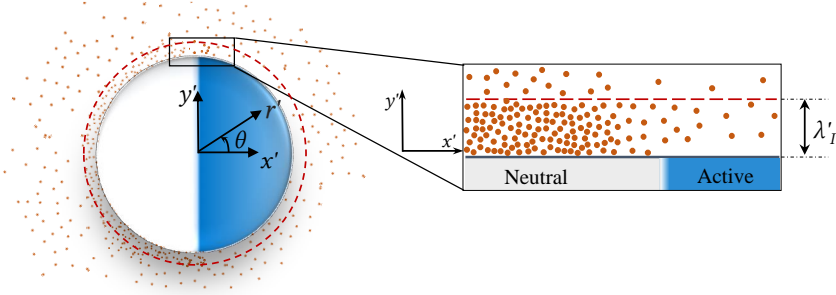


Figure 1: Schematic of an axisymmetric Janus particle suspended in a non-Newtonian medium with a uniform external solute concentration. Zoomed-in view shows the solute in the thin interaction layer above a surface with varying activity. λ_I' is the interaction layer thickness.

a second-order fluid and Carreau model to capture the weak non-Newtonian effects. The analysis, however, was carried out by assuming the slip to be that in a Newtonian medium, which leaves the understanding of hydrodynamics of Janus particles incomplete.

In the context of electrophoresis, it has been shown that the modification in slip due to complex rheology can significantly alter the particle motion and flow field around it (Khair *et al.* 2012). Analogously, we ask: can fluid rheology significantly alter the diffusio-osmotic slip over an active surface and affect the motion of a Janus particle? Furthermore, FEM based numerical simulations of Natale *et al.* (2017) demonstrated the presence of an extensional flow across the point of discontinuity in the surface activity, triggered due to large gradients in viscoelastic stresses. But it is currently unknown as to how is this related to the external concentration field which drives the flow.

In this work, we study the influence of viscoelasticity (second-order-fluid model) and shear-thinning/thickening (Carreau-fluid model) on the slip and mobility of an axisymmetric Janus particle. Using matched asymptotic expansions, we provide an analytical expression for the modification of the diffusio-osmotic slip. Employing the reciprocal theorem, we evaluate the modification in the swimming velocity from that reported by Datt *et al.* (2015, 2017). Since our results are applicable to a general diffusio-osmotic flow of a complex fluid, they can be used to model transport of biological fluids through narrow channels and confinements, where applying pressure drop is undesirable (Michelin *et al.* 2015; Lisicki *et al.* 2016; Michelin & Lauga 2019).

2. Active particle in a second-order-fluid

The non-Newtonian fluid surrounding the active particle consists of a solute of uniform concentration (C'_∞). The solute, treated as a continuum, interacts with an active particle of radius a' . The short-range interaction is governed by

$$\Phi'(r, \theta) = k'_B T' \psi(r, \theta), \quad (2.1)$$

which acts over the length scale λ_I' , where $\lambda_I' \ll a'$. Here $'$ denotes the dimensional variables. This interaction generates a pressure in the thin interaction layer (which induces a potential-force $\nabla' \Phi'$) and decays to zero far away from the surface. The particle surface is partially active; a fixed-flux adsorption (\mathcal{A}') varies in the tangential direction as a step function. Since the interaction layer (λ_I') is very thin compared to the particle radius (a'), we model the particle-layer system as a flat-plate system (see fig.1). This approximation introduces an error of $\mathcal{O}(\lambda_I'/a')$ and has been employed earlier in studies involving particle electrophoresis (Anderson 1989; O'Brien 1983). Following Michelin &

Lauga (2014), we represent the system using the following non-dimensional equations

$$\nabla \cdot \mathbf{u} = 0, \quad -\nabla p + \nabla^2 \mathbf{u} + De \nabla \cdot \mathbf{S} - \frac{1}{\epsilon^2} (c + C_\infty) \nabla \psi = \mathbf{0}, \quad (2.2a)$$

$$Pe(\mathbf{u} \cdot \nabla c) = \nabla \cdot [\nabla c + (c + C_\infty) \nabla \psi]. \quad (2.2b)$$

The characteristic scales are

$$C_{ch} = \frac{|\mathcal{A}'|a'}{D'}, \quad U_{ch} = \frac{k'_B T' \lambda_I'^2 C_{ch}}{\mu' a'}, \quad p_{ch} = \frac{\mu' U_{ch}}{a'}, \quad y_{ch} = x_{ch} = a'. \quad (2.3)$$

Here, D' is the solute diffusion coefficient, c denotes the disturbance to the uniform concentration C_∞ (defined as: $c = C - C_\infty$). In eq. (2.2a), the polymeric stress $\mathbf{S} = \mathbf{A} \cdot \mathbf{A} + \delta \mathbf{B}$, where \mathbf{A} is the rate of strain tensor ($\nabla \mathbf{u} + (\nabla \mathbf{u})^T$) and \mathbf{B} is the steady-state Rivlin-Ericksen tensor (Bird *et al.* 1987; Ho & Leal 1976). The dimensionless quantities are defined as

$$Pe = \frac{U_{ch} a'}{D'}, \quad De = \frac{\Psi'_1 + \Psi'_2}{\mu'} \left(\frac{U_{ch}}{a'} \right), \quad \delta = \frac{-\Psi'_1}{2(\Psi'_1 + \Psi'_2)} \text{ and } \epsilon = \frac{\lambda_I'}{a'}, \quad (2.4)$$

where Pe (Peclet number) is the ratio of diffusive to advective time scales; De (Deborah number) defines the ratio of viscoelastic time scale to that based on shear arising due to macro-scale particle movement; δ is a viscometric parameter which compares first and second normal stress coefficients; ϵ is the dimensionless thickness of the interaction layer.

The boundary conditions are

$$\left(\frac{\partial c}{\partial y} \Big|_{y=0} + (c + C_\infty) \frac{\partial \psi}{\partial y} \Big|_{y=0} \right) = \frac{\mathcal{A}'(x')}{|\mathcal{A}'|} = \mathcal{K}(x) \quad \text{and} \quad \mathbf{u} = \mathbf{0} \quad \text{at} \quad y = 0; \quad (2.5a)$$

$$p \rightarrow 0, \quad \psi \rightarrow 0 \quad \text{and} \quad c \rightarrow 0 \quad \text{as} \quad y \rightarrow \infty. \quad (2.5b)$$

In the next sections, we investigate the influence of non-Newtonian effects on the diffusio-osmotic slip on a partially active surface using matched asymptotic expansions (MAE).

2.1. Matched asymptotic expansions

For an asymptotically thin interaction region ($\epsilon \ll 1$), we expand the field variables (\mathbf{u}, c, p, ψ) as

$$f(x, y) = f^{(0)}(x, y) + \epsilon f^{(1)}(x, y) + \dots \quad (2.6)$$

Following Michelin & Lauga (2014), we divide the domain into an ‘inner’ ($0 \ll y \ll 1$) and ‘outer’ region ($y \gg 1$). We demonstrate that MAE can be used to replace the solution of the inner region with coarse-grained boundary conditions for the outer region.

2.1.1. Outer region

Neglecting the rapidly decaying interaction potential in the outer region i.e. $\psi = 0$ (Michelin & Lauga 2014), the leading order equations read

$$\nabla \cdot \mathbf{u}^{(0)} = 0, \quad -\nabla p^{(0)} + \nabla^2 \mathbf{u}^{(0)} + De \nabla \cdot \mathbf{S}^{(0)} = \mathbf{0}, \quad (2.7a)$$

$$Pe(\mathbf{u}^{(0)} \cdot \nabla c^{(0)}) = \nabla^2 c^{(0)}, \quad (2.7b)$$

subject to the following boundary conditions

$$\mathbf{u}^{(0)} \rightarrow \mathbf{0}, \quad p^{(0)} \rightarrow 0 \quad \text{and} \quad c^{(0)} \rightarrow 0 \quad \text{as} \quad y \rightarrow \infty. \quad (2.8)$$

2.1.2. Inner region

We first rescale the variables to derive the equations in the inner layer. The variables in the inner layer are defined as \hat{f} . In the thin interaction layer limit, using boundary layer principles, we define the characteristic scales for y' – direction, vertical velocity (v') and pressure (p') as λ_I' , ϵU_{ch} and $p_{ch} \epsilon^{-2}$, respectively. Using (2.6) and (2.2), we obtain the leading order equations in the inner region

$$\frac{\partial \hat{u}^{(0)}}{\partial \hat{x}} + \frac{\partial \hat{v}^{(0)}}{\partial \hat{y}} = 0, \quad (2.9a)$$

$$-\frac{\partial \hat{p}^{(0)}}{\partial \hat{x}} + \frac{\partial^2 \hat{u}^{(0)}}{\partial \hat{y}^2} + De \left(\frac{\partial \hat{S}_{xx}^{(0)}}{\partial \hat{x}} + \frac{\partial \hat{S}_{yx}^{(0)}}{\partial \hat{y}} \right) = (c^{(0)} + C_\infty) \frac{\partial \hat{\psi}^{(0)}}{\partial \hat{x}}, \quad (2.9b)$$

$$-\frac{\partial \hat{p}^{(0)}}{\partial \hat{y}} + De \left(\frac{\partial \hat{S}_{yy}^{(0)}}{\partial \hat{y}} \right) = (c^{(0)} + C_\infty) \frac{\partial \hat{\psi}^{(0)}}{\partial \hat{y}}, \quad (2.9c)$$

$$\epsilon^2 Pe \left(\hat{u}^{(0)} \frac{\partial \hat{c}^{(0)}}{\partial \hat{x}} + \hat{v}^{(0)} \frac{\partial \hat{c}^{(0)}}{\partial \hat{y}} \right) = \frac{\partial}{\partial \hat{y}} \left(\frac{\partial \hat{c}^{(0)}}{\partial \hat{y}} + (\hat{c}^{(0)} + C_\infty) \frac{\partial \hat{\psi}^{(0)}}{\partial \hat{y}} \right), \quad (2.9d)$$

subject to the following boundary conditions at the leading order

$$\mathbf{u}^{(0)} \Big|_{\hat{y}=0} = \mathbf{0} \quad \text{and} \quad \left(\frac{\partial \hat{c}^{(0)}}{\partial \hat{y}} \Big|_{\hat{y}=0} + (\hat{c}^{(0)} + C_\infty) \frac{\partial \hat{\psi}}{\partial \hat{y}} \Big|_{\hat{y}=0} \right) = 0. \quad (2.10)$$

For low to moderate Pe (i.e. $Pe \ll \epsilon^{-2}$), we can neglect the LHS of (2.9d). This decouples the solute concentration field from the hydrodynamics.

We now perform a perturbation expansion in Deborah number (De) i.e. accounting for weakly non-linear viscoelastic effects such that $\epsilon \ll De \ll 1$. The field variables for each term in (2.6) can be further expanded as

$$f^{(i)}(x, y) = f_0^{(i)}(x, y) + De f_1^{(i)}(x, y) + \dots, \quad (2.11)$$

Here f represents the velocity and pressure field. The concentration field is not expanded in De as, at moderate Pe , it is decoupled from velocity field in the inner region.

$\mathcal{O}(De^0)$ solution: Since our focus is to obtain leading order change in the diffusio-osmotic slip, for convenience, we temporarily drop the superscript (0) from all the variables. The solution to leading order governing equations is

$$\hat{c}(\hat{x}, \hat{y}) = \mathcal{I}(\hat{x}) e^{-\hat{\psi}(\hat{x}, \hat{y})} - C_\infty, \quad \hat{p}_0(\hat{x}, \hat{y}) = \mathcal{I}(\hat{x}) \left(e^{-\hat{\psi}(\hat{x}, \hat{y})} - 1 \right), \text{ and} \quad (2.12a)$$

$$\hat{u}_0(\hat{x}, \hat{y}) = -\mathcal{I}'(\hat{x}) \int_0^{\hat{y}} \int_t^\infty \left(e^{-\hat{\psi}(\hat{x}, s)} - 1 \right) ds dt + \mathcal{J}_0(\hat{x}) \hat{y}. \quad (2.12b)$$

Here $\mathcal{I}(\hat{x})$ and $\mathcal{J}_0(\hat{x})$ are the integration constants, to be determined through matching.

$\mathcal{O}(De^1)$ solution: To obtain the the leading order solution at $\mathcal{O}(De)$, for ease of calculation, we assume the interaction potential ($\hat{\psi}$) to be independent of the tangential direction (x). Solving the equations governing the $\mathcal{O}(De)$ flow, we obtain

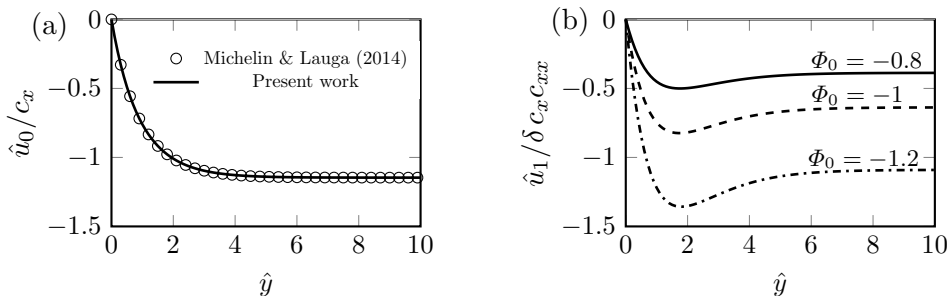


Figure 2: (a) Velocity field of Newtonian fluid inside the interaction layer (for $\Phi_0 = -1$). (b) Normal stress-induced velocity field. The results are for an exponentially decaying solute-surface interaction ($\hat{\psi}(\xi) = \Phi_0 e^{-\xi}$), where a negative Φ_0 represents an attractive interaction.

$$\hat{u}^{(1)} = \mathcal{J}_1(\hat{x})\hat{y} - \delta \mathcal{I}'(\hat{x})\mathcal{I}''(\hat{x}) \int_0^{\hat{y}} dp \int_p^\infty \left\{ \mathcal{G}(r) - \frac{\mathcal{J}_0(\hat{x})}{\mathcal{I}'(\hat{x})} \left(r \mathcal{F}(r) + \int_r^\infty \mathcal{F}(s) ds \right) \right\} dr, \quad (2.13a)$$

$$\text{where } \mathcal{G}(r) = \left\{ \left(\int_r^\infty \mathcal{F}(s) ds \right)^2 + 2\mathcal{F}(r) \left(\int_0^r s\mathcal{F}(s) ds + r \int_r^\infty \mathcal{F}(s) ds \right) - \hat{\psi}'(r) e^{-\hat{\psi}(r)} \left(\int_0^r \left(r - \frac{s}{2} \right) s \mathcal{F}(s) ds + \frac{r^2}{2} \int_r^\infty \mathcal{F}(s) ds \right) \right\}. \quad (2.13b)$$

Here, $\mathcal{F}(\xi) = -1 + e^{-\hat{\psi}(\xi)}$ and $\mathcal{J}_0, \mathcal{J}_1, \mathcal{I}$ are the integration constants. The details of derivation can be found in the supplementary material

2.1.3. Matching

For any field variable f , the matching condition at $\mathcal{O}(\epsilon^0)$ is

$$\lim_{y \rightarrow 0} (f_0^{(0)} + De f_1^{(0)} + \dots) = \lim_{\hat{y} \rightarrow \infty} (\hat{f}_0^{(0)} + De \hat{f}_1^{(0)} + \dots). \quad (2.14)$$

The matching condition on the concentration field (\hat{c}) yields the constant $\mathcal{I}(\hat{x}) = \lim_{y \rightarrow 0} c(x, y)$. We substitute (2.12b) and (2.13) in the above matching condition and find: $\mathcal{J}_0 = \mathcal{J}_1 = 0$ at the leading order. The total slip velocity at the outer edge of the interaction layer is

$$\begin{aligned} \left(u_0^{(0)} + De u_1^{(0)} \right) \Big|_{y=0} &= - \left(\frac{\partial c}{\partial x} \Big|_{y=0} \right) \int_0^\infty \int_t^\infty \left(e^{-\hat{\psi}(s)} - 1 \right) ds dt \\ &\quad - De \delta \left(\frac{\partial c}{\partial x} \Big|_{y=0} \frac{\partial^2 c}{\partial x^2} \Big|_{y=0} \right) \int_0^\infty dp \int_p^\infty \mathcal{G}(r) dr. \end{aligned} \quad (2.15)$$

Modification to the diffusio-osmotic slip velocity (arising from the non-Newtonian effects) is found to be proportional to the first and second derivative (in the tangential direction) of the bulk-scale concentration at the particle *surface*. The above result is also applicable to diffusio-osmotic flows in microchannels arising from externally imposed concentration gradients (Anderson *et al.* 1982). The proportionality to $De \delta$ and the definitions described in (2.3) suggests that the effect of viscoelasticity is solely due to first normal stress difference. Furthermore, a dimensional form of the slip velocity reveals

that the first order slip has a dependency on the characteristic length scale, whereas the Newtonian slip is independent of it.

Fig. 2(a) shows the Newtonian component of the velocity field ($\hat{u}_0^{(0)}$) inside the thin interaction layer for an exponentially decaying solute-surface attraction (Sharifi-Mood *et al.* 2013). Our prediction matches exactly with that reported by Michelin & Lauga (2014). Fig. 2(b) shows the viscoelastic component of the velocity field ($\hat{u}_1^{(0)}$) inside the thin interaction layer. The curve undergoes a minimum before approaching an asymptotic value, which intensifies as the attraction between the solute and the surface increases.

2.2. Diffusio-osmotic slip on an active particle

We now apply the results of previous section to a spherical Janus particle i.e. the tangential direction is polar angle θ , varying from 0 to π . The surface activity \mathcal{K} follows a step function

$$\mathcal{K} = \begin{cases} 1 & \theta < \theta_c \\ 0 & \theta > \theta_c, \end{cases} \quad (2.16)$$

where θ_c is the angle at which the activity undergoes a step change i.e. surface coverage of the activity. To evaluate the flow field inside the thin interaction layer, we require solution to the concentration field (c) in the outer region. In the absence of advection ($Pe = 0$), the solution to (2.7b) is sought in terms of an expansion in Legendre polynomials. Following Golestanian *et al.* (2007), we obtain the solution to bulk-scale concentration field as

$$c(r, \theta) = \sum_{n=0}^{\infty} \frac{-\mathcal{K}_n}{(n+1)} \frac{P_n(\cos \theta)}{r^{n+1}}, \quad (2.17)$$

where P_n is the n th Legendre polynomial. \mathcal{K}_n are the spectral coefficients of the activity distribution ($\mathcal{K}(\theta) = \sum_{n=0}^{\infty} \mathcal{K}_n P_n(\cos \theta)$), which can be found by taking an inner product with Legendre polynomials. Simplifying, we get

$$\mathcal{K}_0 = \frac{(1 - \cos \theta_c)}{2} \quad \text{and} \quad \mathcal{K}_n = \frac{-1}{2} (P_{n+1}(\cos \theta_c) - P_{n-1}(\cos \theta_c)) \quad \text{for } n \geq 1. \quad (2.18)$$

Using the solution to the disturbance concentration (2.17), we obtain the total slip velocity for any surface coverage (θ_c). Fig. 3(a) shows the total bulk-scale slip velocity (solid line) varying across the polar angle for three different surface coverage ($\theta_c = \pi/4, \pi/2, 3\pi/4$). The dashed line shows the slip velocity for a Newtonian fluid. The negative sign depicts that the diffusio-osmotic flow is towards the active region. For a second-order fluid, the figure depicts a localized reversal of slip velocity across θ_c . For any surface coverage, the slip velocity exhibits sharp non-linear gradients at θ_c . Natale *et al.* (2017) also reported such behavior in viscoelastic stresses at θ_c in their FEM simulations. They reported an extensional flow, triggered by large viscoelastic stresses, across the point of discontinuity in surface activity.

To analyze this slip reversal, we study the behavior of concentration field around the particle as the slip (2.15) depends on the first and second polar gradient of the concentration field. In fig. 3(b,c), c , c_θ and $c_{\theta\theta}$ profiles are shown for $\theta_c = \pi/2$. A step change in surface activity causes the second gradient to undergo a sharp change at $\theta = \theta_c$, which is also reflected in the slip velocity. The evaluation of $c_{\theta\theta}$, accounting for first 700 modes, exhibits oscillations near the point of discontinuity of surface activity. This can be averted by approximating (2.16) as a sigmoidal function. Refer to the supplementary material for additional details.

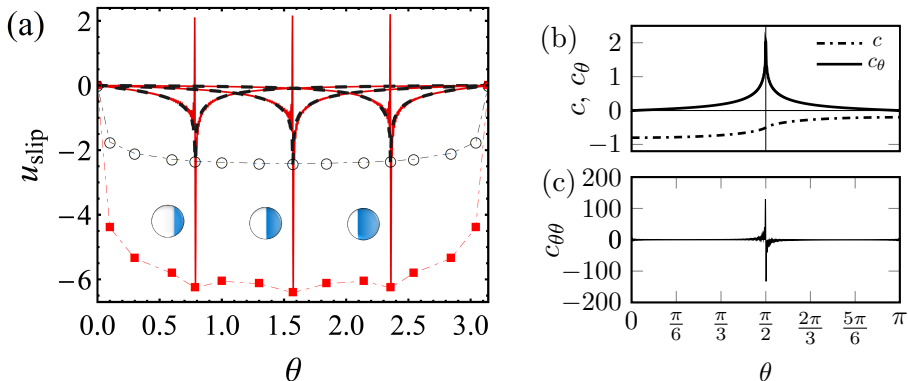


Figure 3: (a) The solid red line represents the total slip velocity (for three different surface coverage) along the polar angle for $\hat{\psi}(\xi) = -e^{-\xi}$, $De = 0.05$, and $\delta = -0.5$. The dashed line represents the Newtonian slip velocity. The markers represent the maximum magnitude of the slip velocity for a range of surface coverage: $\theta_c \in (0, \pi)$: empty circles represent the Newtonian case; solid squares represent the second-order fluid. (b) Concentration profile and its gradient along the polar angle on particle surface for $\theta_c = \pi/2$. (c) shows the profile for $c_{\theta\theta}$. Note that due to computational cost, first 700 modes were used to describe the concentration field and its gradients.

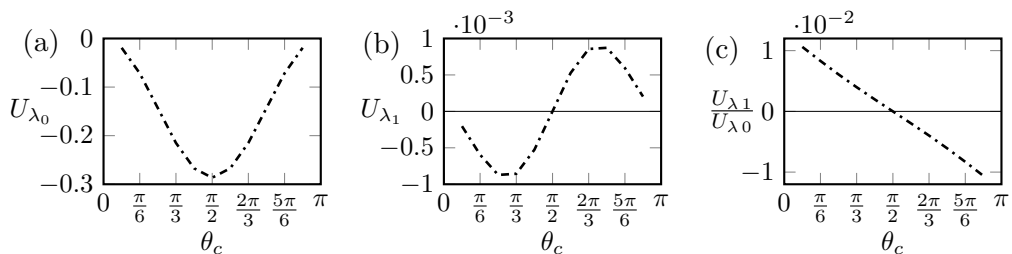


Figure 4: (a) Variation of swimming velocity due to Newtonian surface slip (U_{λ_0}) for various surface coverages. (b) Perturbation to swimming velocity due to modification in the slip (U_{λ_1}). (c) Ratio of the swimming velocity components i.e. (b) and (a). It should be noted that swimming velocity remains converged for $n > 100$. Parameters: $De = 0.05$, $\delta = -0.5$, and $\phi_0 = -1$.

2.2.1. Swimming velocity

The motion of the active sphere is found by using reciprocal theorem. Following Stone & Samuel (1996) and Ho & Leal (1976), we obtain

$$U = \frac{-1}{4\pi} \int_{S_p} (\mathbf{u}_0 + De \mathbf{u}_1)|_{r=1} \cdot \mathbf{e}_x dS - \frac{1}{6\pi} De \int_{V_f} \mathbf{S}_0 : \nabla \mathbf{u}^t dV. \quad (2.19)$$

Here, \mathbf{u}^t is the test flow field which governs the motion of a rigid sphere in x -direction with unit velocity (Michelin & Lauga 2014; Datt *et al.* 2015), and \mathbf{S}_0 is the polymeric stress. The first integral (U_λ) denotes the contribution to swimming velocity arising from the slip, which contains a Newtonian (U_{λ_0}) and non-Newtonian (U_{λ_1}) component. The second integral (U_B) accounts for the contribution from polymeric stresses in the bulk.

In their evaluation of swimming velocity, Datt *et al.* (2017) accounted for the bulk viscoelastic effects, assuming the surface slip to be that of Newtonian fluid i.e. neglecting U_{λ_1} . Upon substituting the slip velocity into (2.19), we find U_{λ_0} and U_{λ_1} and compare them in fig. 4 for different surface coverage. The correction to the swimming velocity is minor and changes sign with the surface coverage; swimming velocity increases for

$\theta_c < \pi/2$ and reduces for $\theta_c > \pi/2$ as compared to that in a Newtonian fluid. The magnitude of correction to swimming velocity suggests that the results obtained by Datt *et al.* (2017) are reasonably accurate. Although the modification in the slip velocity (2.15) does not significantly affect the bulk-scale motion, it provides an estimate of the hydrodynamic disturbance, which can be used to accurately model the interaction active particles in viscoelastic fluids (Patterson *et al.* 2016; Rallabandi *et al.* 2019).

3. Active particle in a shear-thinning fluid

The equation governing a weak shear-thinning flow is described by

$$\nabla' \cdot \mathbf{u}' = 0, \quad -\nabla' p' + \nabla' \cdot (\mu' \mathbf{A}') - C' \nabla' \Phi' = 0. \quad (3.1)$$

The viscosity follows a general non-linear relation with respect to Newtonian shear-rate (γ_0) (Khair *et al.* 2012): $\mu' = \mu'_0 (1 + \chi \mu_1(\gamma_0))$. Here, χ is a small parameter which determines the viscosity ratio (Datt *et al.* 2015). The variables are non-dimensionalized as in §2. We use matched asymptotic expansion (assuming $Pe \ll \epsilon^{-2}$ and $\epsilon \ll 1$) and perturbation expansion (in χ) to obtain the leading order slip for a generalized weakly shear-thinning fluid:

$$\begin{aligned} \left(u_0^{(0)} + \chi u_1^{(0)} \right) \Big|_{y=0} &= -c_\theta(1, \theta) \int_0^\infty \int_t^\infty \left(e^{-\hat{\psi}(s)} - 1 \right) ds dt \\ &+ \chi c_\theta(1, \theta) \int_0^\infty \mu_1 \left(\gamma_0^{(0)} \right) \int_t^\infty \left(e^{-\hat{\psi}(s)} - 1 \right) ds dt. \end{aligned} \quad (3.2)$$

Since the power-law model diverges for asymptotically small shear-rates (Bird *et al.* 1987), we choose the Carreau model to capture viscosity variation: $\mu_1(\gamma_0) = (1 + \tau^2 \gamma_0^2)^{\frac{n-1}{2}} - 1$. Here τ is the fluid relaxation time scale and n characterizes the degree of shear-thinning ($n < 1$) or thickening ($n > 1$). The correction to Newtonian slip is

$$\chi \hat{u}_1^{(0)} \Big|_{y=0} = \chi c' (1, \theta) \int_0^\infty \left[\left(1 + Cu_\lambda^2 c_\theta(1, \theta)^2 \left(\int_t^\infty \mathcal{F}(t) \right)^2 \right)^{\frac{n-1}{2}} - 1 \right] \int_t^\infty \mathcal{F}(s) ds dt, \quad (3.3)$$

where $\mathcal{F}(\xi) = -1 + e^{-\hat{\psi}(\xi)}$ and Cu_λ (Carreau number based on shear in the interaction layer) is the ratio of timescales associated with relaxation (τ) and shear in the flow (λ'_I/U_{ch}). This is different than the Carreau number in the bulk of the fluid, as defined by Datt *et al.* (2017). Using (3.2) and (3.3), we numerically evaluate the slip for $n = 0.25$ and depict its variation along the particle surface in fig. 5 (a). For high Carreau numbers ($Cu_\lambda \sim 10^2$), we find a modest increase in the total slip velocity. Since the shear in the thin interaction layer is generally high (i.e. $U_{ch}/\lambda'_I \gg \mathcal{O}(1)$) and relaxation time scales of biological fluids are $\mathcal{O}(1)$ (Zare *et al.* 2019), such large Carreau number is possible.

We further evaluate the swimming velocity using the reciprocal theorem as:

$$U = \frac{-1}{4\pi} \int_{S_p} (\mathbf{u}_0 + \chi \mathbf{u}_1) \Big|_{r=1} \cdot \mathbf{e}_x dS - \frac{1}{6\pi} \chi \int_{V_f} \mu(\gamma_0) \mathbf{A}_0 : \nabla \mathbf{u}^t dV. \quad (3.4)$$

Similar to §2.2.1, the first integral contains the Newtonian (U_{λ_0}) and non-Newtonian (U_{λ_1}) components. The second integral (U_B) accounts for the bulk stresses arising from viscosity variations. Neglecting U_{λ_1} , Datt *et al.* (2017) reported that a self-propelling Janus particle always swims slower in a Carreau-fluid (i.e. U_B opposes U_{λ_0}). Substituting (3.3) in (3.4) and integrating numerically, we find that the contribution from U_{λ_1}

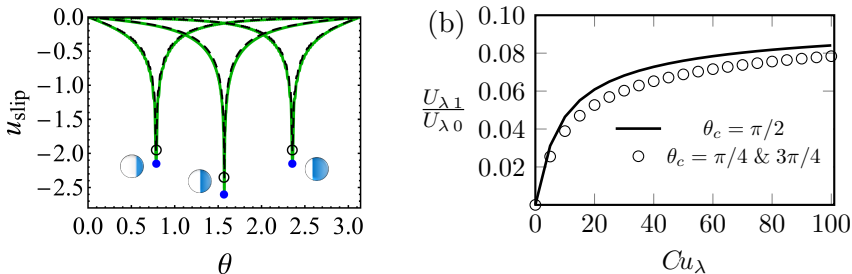


Figure 5: (a) The solid line represents the variation of total slip velocity along the polar angle for $\hat{\psi}(\xi) = -e^{-\xi}$ and $Cu_{\lambda} = 100$. The dashed line represents the Newtonian slip velocity. The empty and filled markers represent the absolute maximum slip velocity in Newtonian and Carreau fluid, respectively. (b) Variation of swimming velocity (arising from the surface slip) with Cu_{λ} , for three different surface coverage (θ_c). Other parameters: $\chi = 0.1$, $n = 1/4$.

modestly affects the swimming of a Janus particle. This is shown in figure 5(b) for three different surface coverages. The positive sign shows that $U_{\lambda 1}$ adds to the contribution arising from the Newtonian slip (contrary to U_B as reported by Datt *et al.* (2017)).

4. Conclusion

The results of the current study reveal the effects of fluid rheology on the diffusio-osmotic slip over an active surface and its consequence on the mobility of a Janus particle. Using matched asymptotic expansions in conjunction with perturbation theory, we derived the modification to slip velocity for a second-order fluid. Our result (eq.2.15), for an axisymmetrically active Janus particle, show that the normal stresses significantly alter the slip velocity. The proportionality to second tangential gradient results in a sharp reversal of the surface slip, triggered by large polymeric stresses across the discontinuity of surface activity. This explains the generation of extensional flows across a step change in activity observed by Natale *et al.* (2017). Using the reciprocal theorem, we found that the modification in the slip does not have a pronounced effect on the swimming velocity and is therefore determined primarily by the Newtonian slip and bulk polymeric stresses.

We further applied our framework to a generalized weakly shear-thinning fluid and obtained the modification to slip velocity (see eq.3.2). Employing a Carreau-fluid model, we showed that shear-thinning effects marginally increase the slip velocity, provided the time scale associated with the shear in the interaction layer is asymptotically smaller than the fluid relaxation time. Using the reciprocal theorem, we showed a modest enhancement in the swimming velocity for all surface coverages.

Another key implication of our results is that it provides a precise estimate of the hydrodynamic disturbance around an active particle. This hence can be of great significance towards accurate modeling of the interaction of two or more active particles in viscoelastic fluids (Rallabandi *et al.* 2019). Recently, Michelin *et al.* (2015); Michelin & Lauga (2019) have designed ‘phoretic pumps’ which can transport the fluid without the need of applying pressure difference across the channel. This can be helpful in transportation of biological fluids through narrow channels. The flow in such systems occurs due to local concentration gradients, arising either from geometric variation (Lisicki *et al.* 2016; Michelin *et al.* 2015) or variation in surface activity (Michelin & Lauga 2019). Since our results are applicable to a general diffusio-osmotic slip, they should be useful to model flow of complex fluids through such pumps.

REFERENCES

- ANDERSON, JL, LOWELL, ME & PRIEVE, DC 1982 Motion of a particle generated by chemical gradients part I. non-electrolytes. *Journal of Fluid Mechanics* **117**, 107–121.
- ANDERSON, JOHN L 1989 Colloid transport by interfacial forces. *Annual review of fluid mechanics* **21** (1), 61–99.
- BIRD, ROBERT BYRON, ARMSTRONG, ROBERT CALVIN & HASSAGER, OLE 1987 Dynamics of polymeric liquids. vol. 1: Fluid mechanics .
- BRADY, JOHN F 2011 Particle motion driven by solute gradients with application to autonomous motion: continuum and colloidal perspectives. *Journal of Fluid Mechanics* **667**, 216–259.
- DATT, CHARU, NATALE, GIOVANNANTONIO, HATZIKIRIAKOS, SAVVAS G & ELFRING, GWYNN J 2017 An active particle in a complex fluid. *Journal of Fluid Mechanics* **823**, 675–688.
- DATT, CHARU, ZHU, LAILAI, ELFRING, GWYNN J & PAK, ON SHUN 2015 Squirming through shear-thinning fluids. *Journal of Fluid Mechanics* **784**.
- GAO, WEI & WANG, JOSEPH 2014 Synthetic micro/nanomotors in drug delivery. *Nanoscale* **6** (18), 10486–10494.
- GOLESTANIAN, R, LIVERPOOL, TB & AJDARI, A 2007 Designing phoretic micro-and nano-swimmers. *New Journal of Physics* **9** (5), 126.
- GOLESTANIAN, RAMIN, LIVERPOOL, TANNIEMOLA B & AJDARI, ARMAND 2005 Propulsion of a molecular machine by asymmetric distribution of reaction products. *Physical review letters* **94** (22), 220801.
- GOMEZ-SOLANO, JUAN RUBEN, BLOKHUIS, ALEX & BECHINGER, CLEMENS 2016 Dynamics of self-propelled janus particles in viscoelastic fluids. *Physical review letters* **116** (13), 138301.
- HO, BP & LEAL, LG 1976 Migration of rigid spheres in a two-dimensional unidirectional shear flow of a second-order fluid. *Journal of Fluid Mechanics* **76** (4), 783–799.
- KHAIR, ADITYA S, POSLUSZNY, DENISE E & WALKER, LYNN M 2012 Coupling electrokinetics and rheology: electrophoresis in non-newtonian fluids. *Physical Review E* **85** (1), 016320.
- LISICKI, MACIEJ, MICHELIN, SÉBASTIEN & LAUGA, ERIC 2016 Phoretic flow induced by asymmetric confinement. *Journal of Fluid Mechanics* **799**.
- MICHELIN, SÉBASTIEN & LAUGA, ERIC 2014 Phoretic self-propulsion at finite pécelet numbers. *Journal of Fluid Mechanics* **747**, 572–604.
- MICHELIN, SÉBASTIEN & LAUGA, ERIC 2019 Universal optimal geometry of minimal phoretic pumps. *Scientific reports* **9** (1), 10788.
- MICHELIN, SÉBASTIEN, MONTENEGRO-JOHNSON, THOMAS D, DE CANIO, GABRIELE, LOBATO-DAUZIER, NICOLAS & LAUGA, ERIC 2015 Geometric pumping in autophoretic channels. *Soft matter* **11** (29), 5804–5811.
- NATALE, GIOVANNANTONIO, DATT, CHARU, HATZIKIRIAKOS, SAVVAS G & ELFRING, GWYNN J 2017 Autophoretic locomotion in weakly viscoelastic fluids at finite pécelet number. *Physics of Fluids* **29** (12), 123102.
- O'BRIEN, RW 1983 The solution of the electrokinetic equations for colloidal particles with thin double layers. *Journal of Colloid and Interface Science* **92** (1), 204–216.
- PATTESON, ALISON E, GOPINATH, ARVIND & ARRATIA, PAULO E 2016 Active colloids in complex fluids. *Current Opinion in Colloid & Interface Science* **100** (21), 86–96.
- PIETRZYK, KYLE, NGANGUIA, HERVE, DATT, CHARU, ZHU, LAILAI, ELFRING, GWYNN J & PAK, ON SHUN 2019 Flow around a squirmer in a shear-thinning fluid. *Journal of Non-Newtonian Fluid Mechanics* **268**, 101–110.
- RALLABANDI, BHARGAV, YANG, FAN & STONE, HOWARD A 2019 Motion of hydrodynamically interacting active particles. *arXiv preprint arXiv:1901.04311* .
- SHARIFI-MOOD, NIMA, KOPLIK, JOEL & MALDARELLI, CHARLES 2013 Diffusiophoretic self-propulsion of colloids driven by a surface reaction: the sub-micron particle regime for exponential and van der waals interactions. *Physics of Fluids* **25** (1), 012001.
- STONE, HOWARD A & SAMUEL, ARAVINTHAN DT 1996 Propulsion of microorganisms by surface distortions. *Physical review letters* **77** (19), 4102.
- WEISSTEIN, ERIC W 2002 Legendre polynomial. *Wolfram Research, Inc.* (<http://mathworld.wolfram.com/LegendrePolynomial.html>) .
- ZARE, YASSER, PARK, SANG PHIL & RHEE, KYONG YOP 2019 Analysis of complex viscosity and shear thinning behavior in poly (lactic acid)/poly (ethylene oxide)/carbon nanotubes biosensor based on carreau–yasuda model. *Results in Physics* **13**, 102245.

Supplementary Material

Akash Choudhary,¹ T. Renganathan¹, and S. Pushpavanam^{1,†}

¹*Department of Chemical Engineering, Indian Institute of Technology Madras, Chennai, 600036 TN, India*

In this Supplementary Material we provide details of the derivation of slip velocity and its validation with literature. In section A, we detail the treatment of the equations in the inner region. Later we describe the matching of solutions. In section B, we validate our results with those reported by Michelin & Lauga (2014) for Newtonian fluid. In section C, we show the effect of approximating the step change in the surface activity, as a smooth sigmoidal function, on the surface slip.

S.1 Derivation of slip velocity

S.1.1 Equations in the inner region

The components of the polymeric stress tensor (\mathbf{S}) are rescaled as:

$$S_{xx} = \frac{\hat{S}_{xx}}{\epsilon^2} = \frac{1}{\epsilon^2} \left(\frac{\partial \hat{u}}{\partial \hat{y}} \right)^2, \quad S_{yy} = \frac{\hat{S}_{yy}}{\epsilon^2} = \frac{1}{\epsilon^2} (1 + 2\delta) \left(\frac{\partial \hat{u}}{\partial \hat{y}} \right)^2, \quad (\text{S1a})$$

$$S_{xy} = S_{yx} = \frac{\hat{S}_{xy}}{\epsilon} = \frac{\hat{S}_{yx}}{\epsilon} = \frac{2\delta}{\epsilon} \left(\frac{\partial \hat{u}}{\partial \hat{y}} \frac{\partial \hat{u}}{\partial \hat{x}} + \frac{\hat{v} \frac{\partial^2 \hat{u}}{\partial \hat{y}^2} + \hat{u} \frac{\partial^2 \hat{u}}{\partial \hat{y} \partial \hat{x}}}{2} \right). \quad (\text{S1b})$$

$\mathcal{O}(De^0)$ solution: Since our focus is to obtain leading order change in the diffusio-osmotic slip, for convenience, we temporarily drop the superscript (0) from all the variables. The solution to leading order governing equations ($\hat{g}_0^{(0)}$) is

$$\hat{c}(\hat{x}, \hat{y}) = \mathcal{I}(\hat{x}) e^{-\hat{\psi}(\hat{x}, \hat{y})} - C_\infty, \quad \hat{p}_0(\hat{x}, \hat{y}) = \mathcal{I}(\hat{x}) \left(e^{-\hat{\psi}(\hat{x}, \hat{y})} - 1 \right), \text{ and} \quad (\text{S2a})$$

$$\hat{u}_0(\hat{x}, \hat{y}) = -\mathcal{I}'(\hat{x}) \int_0^{\hat{y}} \int_t^\infty \left(e^{-\hat{\psi}(\hat{x}, s)} - 1 \right) ds dt + \mathcal{J}_0(\hat{x}) \hat{y}. \quad (\text{S2b})$$

Here $\mathcal{I}(\hat{x})$ and $\mathcal{J}_0(\hat{x})$ are the integration constants, which are determined using the matching conditions. The leading order velocity field is represented in a different form than that reported by Michelin & Lauga (2014), to help us later in the calculations.

$\mathcal{O}(De^1)$ solution: To obtain the the leading order solution at $\mathcal{O}(De)$, for ease of calculation/simplicity, we assume the interaction potential to be independent of tangential direction (i.e. $\hat{\psi}(\hat{y})$). The flow field at $\mathcal{O}(De)$ is governed by

$$\frac{\partial \hat{u}^{(1)}}{\partial \hat{x}} + \frac{\partial \hat{v}^{(1)}}{\partial \hat{y}} = 0, \quad (\text{S3a})$$

$$-\frac{\partial \hat{p}^{(1)}}{\partial \hat{x}} + \frac{\partial^2 \hat{u}^{(1)}}{\partial \hat{y}^2} + \frac{\partial \hat{S}_{xx}^{(0)}}{\partial \hat{x}} + \frac{\partial \hat{S}_{xy}^{(0)}}{\partial \hat{y}} = 0, \quad (\text{S3b})$$

$$-\frac{\partial \hat{p}^{(1)}}{\partial \hat{y}} + \frac{\partial \hat{S}_{yy}^{(0)}}{\partial \hat{y}} = 0. \quad (\text{S3c})$$

Using the pressure decay condition ($\hat{p} \rightarrow 0$), the solution to (S3c) yields $\hat{p}_1 = \hat{S}_{yy}^{(0)}$.

Substituting \hat{p}_1 in (S3b) and simplifying, we obtain

$$\frac{\partial^2 \hat{u}_1}{\partial \hat{y}^2} = -\delta \left\{ -\frac{\partial \hat{u}_0}{\partial \hat{y}} \frac{\partial^2 \hat{u}_0}{\partial \hat{y} \partial \hat{x}} + \frac{\partial \hat{u}_0}{\partial \hat{x}} \frac{\partial^2 \hat{u}_0}{\partial \hat{y}^2} + \hat{v}_0 \frac{\partial^3 \hat{u}_0}{\partial \hat{y}^3} + \hat{u}_0 \frac{\partial^3 \hat{u}_0}{\partial \hat{x} \partial \hat{y}^2} \right\}. \quad (\text{S4})$$

Here, \hat{v}_0 is found by substituting (S2b) in the continuity equation and integrating it over \hat{y} direction.

Substituting (S2) and \hat{v}_0 into the above equation, and integrating twice over \hat{y} direction and using the boundary conditions, we obtain

$$\begin{aligned} \hat{u}^{(1)} = \mathcal{J}_1(\hat{x})\hat{y} - \delta \mathcal{I}'(\hat{x})\mathcal{I}''(\hat{x}) \int_0^{\hat{y}} dp \int_p^\infty & \left\{ \left(\int_r^\infty \mathcal{F}(s) ds \right)^2 + 2\mathcal{F}(r) \left(\int_0^r s\mathcal{F}(s) ds + r \int_r^\infty \mathcal{F}(s) ds \right) \right. \\ & - \hat{\psi}'(r) e^{-\hat{\psi}(r)} \left(\int_0^r \left(r - \frac{s}{2} \right) s \mathcal{F}(s) ds + \frac{r^2}{2} \int_r^\infty \mathcal{F}(s) ds \right) \\ & \left. - \frac{\mathcal{J}_0(\hat{x})}{\mathcal{I}'(\hat{x})} \left(r \mathcal{F}(r) + \int_r^\infty \mathcal{F}(s) ds \right) \right\} dr. \quad (\text{S5}) \end{aligned}$$

The evaluation of the above solution is simplified by changing the order of integration. We use of the following simplifications:

$$\begin{aligned} 2\mathcal{F}(r) \left(\int_0^r \int_t^\infty \mathcal{F}(s) ds dt \right) dr &= 2\mathcal{F}(r) \left(\int_0^r s\mathcal{F}(s) ds + r \int_r^\infty \mathcal{F}(s) ds \right) dr \text{ and} \\ \int_0^r \int_0^\omega \int_t^\infty \mathcal{F}(s) ds dt d\omega &= \int_0^r \left(r - \frac{s}{2} \right) s \mathcal{F}(s) ds + \frac{r^2}{2} \int_r^\infty \mathcal{F}(s) ds. \end{aligned}$$

Here, $\mathcal{F}(\xi) = -1 + e^{\hat{\psi}(\xi)}$, \mathcal{J}_0 , \mathcal{J}_1 , and \mathcal{I} are the integration coefficients, to be determined through matching.

S.1.2 Matching

For any field variable f , the matching condition at $\mathcal{O}(\epsilon^0)$ is

$$\lim_{y \rightarrow 0} (f_0^{(0)} + De f_1^{(0)} + \dots) = \lim_{\hat{y} \rightarrow \infty} (\hat{f}_0^{(0)} + De \hat{f}_1^{(0)} + \dots). \quad (\text{S6})$$

Since $y \rightarrow 0$ in LHS, we use Taylor series and obtain

$$\left(f_0^{(0)} \Big|_{y=0} + y \frac{\partial f_0^{(0)}}{\partial y} \Big|_{y=0} \right) + De \left(f_1^{(0)} \Big|_{y=0} + y \frac{\partial f_1^{(0)}}{\partial y} \Big|_{y=0} \right) + \dots = \lim_{\hat{y} \rightarrow \infty} [\hat{f}_0^{(0)} + De \hat{f}_1^{(0)} + \dots].$$

The matching condition on the concentration field (\hat{c}) yields the constant $\mathcal{I}(\hat{x}) = \lim_{y \rightarrow 0} c(x, y)$. To obtain \mathcal{J}_0 and \mathcal{J}_1 , we substitute (S2b) and (S5) in the matching condition (S7). At the leading order, we find: $\mathcal{J}_0 = \mathcal{J}_1 = 0$. We obtain the total slip velocity at the outer edge of the interaction layer as

$$\begin{aligned} \left(u_0^{(0)} + De u_1^{(0)} \right) \Big|_{y=0} &= - \left(\frac{\partial c}{\partial x} \Big|_{y=0} \right) \int_0^\infty \int_t^\infty \left(e^{-\hat{\psi}(s)} - 1 \right) ds dt \\ &\quad - De \delta \left(\frac{\partial c}{\partial x} \Big|_{y=0} \frac{\partial^2 c}{\partial x^2} \Big|_{y=0} \right) \int_0^\infty dp \int_p^\infty \mathcal{G}(r) dr. \quad (\text{S7}) \end{aligned}$$

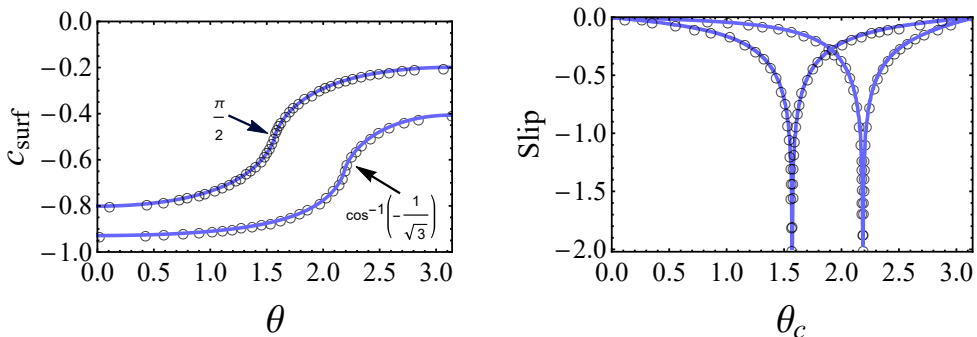


Figure S1: (i) Surface concentration profile and (ii) slip velocity profile for $\cos \theta_c = 0$ and $-1/\sqrt{3}$. The open circles represent the results of Michelin & Lauga (2014) and the mobility coefficient (as defined by Michelin & Lauga (2014)) is fixed to be -1. It should be noted that the mobility coefficient (M) in the main text is -1.1465 (corresponding to $\phi_0 = -1$).

$$\text{Here, } \mathcal{G}(r) = \left\{ \left(\int_r^\infty \mathcal{F}(s) ds \right)^2 + 2\mathcal{F}(r) \left(\int_0^r s\mathcal{F}(s) ds + r \int_r^\infty \mathcal{F}(s) ds \right) - \hat{\psi}'(r) e^{-\hat{\psi}(r)} \left(\int_0^r \left(r - \frac{s}{2} \right) s \mathcal{F}(s) ds + \frac{r^2}{2} \int_r^\infty \mathcal{F}(s) ds \right) \right\}. \quad (\text{S8})$$

S.2 Comparison with the literature

The slip velocity and concentration field for different surface coverage is shown in fig. S1. Our results agree well with that of Michelin & Lauga (2014) (i.e. Newtonian fluid). For the results presented in the main text, we chose first 700 modes to represent the concentration and its gradients. For ease of computation of c_θ and $c_{\theta\theta}$, we used the following recurrence relation Weisstein (2002):

$$\frac{\partial P_n}{\partial \theta} = (P_{n+1} - \cos \theta P_n) \frac{n+1}{\sin \theta}, \quad (\text{S9})$$

where P_n represents the Legendre polynomial of n^{th} mode.

S.3 Sigmoidal function approximation

The step change in surface activity is approximated as a logistic function:

$$\mathcal{K} = 1 / \left(1 + \exp \left[-\zeta \left(\frac{\pi}{2} - \theta \right) \right] \right). \quad (\text{S10})$$

Here ζ determines the sharpness of the transition of activity from 1 to 0. The concentration field and its tangential gradients (at the surface) are depicted in fig.S2(a). The behavior of gradients of the concentration field is qualitatively similar to that reported in main text for a step change. Fig.S2(b) compares the slip velocity for a second-order fluid with that of a Newtonian fluid. Similar to main text, we observe that the polymeric stresses undergo sharp gradients across the transition of activity. The magnitude of the slip is significantly reduced (as compared to that of step change in surface activity) which is a consequence of smooth transition of surface activity.

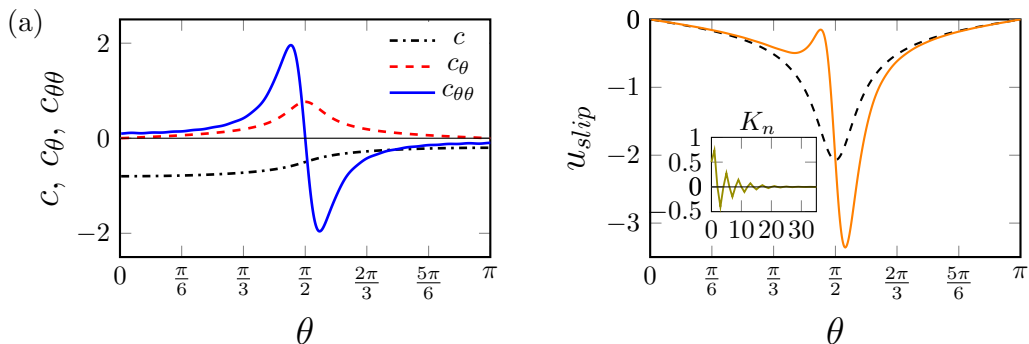


Figure S2: (a) Profile of concentration and its first and second gradient along the polar angle on particle surface for $\theta_c = \pi/2$. (b) The solid line represents the total slip velocity along the polar angle for $\hat{\psi}(\xi) = -2e^{-\xi}$, $\zeta = 15$, $De = 0.5$, and $\delta = -0.5$; dashed line represents the Newtonian slip velocity. The inset shows the rapid convergence of spectral modes.

REFERENCES

- ANDERSON, J.L, LOWELL, M.E & PRIEVE, D.C 1982 Motion of a particle generated by chemical gradients part 1. non-electrolytes. *Journal of Fluid Mechanics* **117**, 107–121.
- ANDERSON, JOHN L 1989 Colloid transport by interfacial forces. *Annual review of fluid mechanics* **21** (1), 61–99.
- BIRD, ROBERT BYRON, ARMSTRONG, ROBERT CALVIN & HASSAGER, OLE 1987 Dynamics of polymeric liquids. vol. 1: Fluid mechanics .
- BRADY, JOHN F 2011 Particle motion driven by solute gradients with application to autonomous motion: continuum and colloidal perspectives. *Journal of Fluid Mechanics* **667**, 216–259.
- DATT, CHARU, NATALE, GIOVANNIANTONIO, HATZIKIRIAKOS, SAVVAS G & ELFRING, GWYNN J 2017 An active particle in a complex fluid. *Journal of Fluid Mechanics* **823**, 675–688.
- DATT, CHARU, ZHU, LAILAI, ELFRING, GWYNN J & PAK, ON SHUN 2015 Squirming through shear-thinning fluids. *Journal of Fluid Mechanics* **784**.
- GAO, WEI & WANG, JOSEPH 2014 Synthetic micro/nanomotors in drug delivery. *Nanoscale* **6** (18), 10486–10494.
- GOLESTANIAN, R, LIVERPOOL, T.B & AJDARI, A 2007 Designing phoretic micro-and nanoswimmers. *New Journal of Physics* **9** (5), 126.
- GOLESTANIAN, RAMIN, LIVERPOOL, TANNIEMOLA B & AJDARI, ARMAND 2005 Propulsion of a molecular machine by asymmetric distribution of reaction products. *Physical review letters* **94** (22), 220801.
- GOMEZ-SOLANO, JUAN RUBEN, BLOKHUIS, ALEX & BECHINGER, CLEMENS 2016 Dynamics of self-propelled janus particles in viscoelastic fluids. *Physical review letters* **116** (13), 138301.
- HO, B.P & LEAL, L.G 1976 Migration of rigid spheres in a two-dimensional unidirectional shear flow of a second-order fluid. *Journal of Fluid Mechanics* **76** (4), 783–799.
- KHAIR, ADITYA S, POSLUSZNY, DENISE E & WALKER, LYNN M 2012 Coupling electrokinetics and rheology: electrophoresis in non-newtonian fluids. *Physical Review E* **85** (1), 016320.
- LISICKI, MACIEJ, MICHELIN, SÉBASTIEN & LAUGA, ERIC 2016 Phoretic flow induced by asymmetric confinement. *Journal of Fluid Mechanics* **799**.
- MICHELIN, SÉBASTIEN & LAUGA, ERIC 2014 Phoretic self-propulsion at finite péclet numbers. *Journal of Fluid Mechanics* **747**, 572–604.
- MICHELIN, SÉBASTIEN & LAUGA, ERIC 2019 Universal optimal geometry of minimal phoretic pumps. *Scientific reports* **9** (1), 10788.
- MICHELIN, SÉBASTIEN, MONTENEGRO-JOHNSON, THOMAS D, DE CANIO, GABRIELE, LOBATO-DAUZIER, NICOLAS & LAUGA, ERIC 2015 Geometric pumping in autophoretic channels. *Soft matter* **11** (29), 5804–5811.
- NATALE, GIOVANNIANTONIO, DATT, CHARU, HATZIKIRIAKOS, SAVVAS G & ELFRING, GWYNN J 2017 Autophoretic locomotion in weakly viscoelastic fluids at finite péclet number. *Physics of Fluids* **29** (12), 123102.

- O'BRIEN, RW 1983 The solution of the electrokinetic equations for colloidal particles with thin double layers. *Journal of Colloid and Interface Science* **92** (1), 204–216.
- PATTESON, ALISON E, GOPINATH, ARVIND & ARRATIA, PAULO E 2016 Active colloids in complex fluids. *Current Opinion in Colloid & Interface Science* **100** (21), 86–96.
- PIETRZYK, KYLE, NGANGUIA, HERVE, DATT, CHARU, ZHU, LAILAI, ELFRING, GWYNN J & PAK, ON SHUN 2019 Flow around a squirmer in a shear-thinning fluid. *Journal of Non-Newtonian Fluid Mechanics* **268**, 101–110.
- RALLABANDI, BHARGAV, YANG, FAN & STONE, HOWARD A 2019 Motion of hydrodynamically interacting active particles. *arXiv preprint arXiv:1901.04311* .
- SHARIFI-MOOD, NIMA, KOPLIK, JOEL & MALDARELLI, CHARLES 2013 Diffusiophoretic self-propulsion of colloids driven by a surface reaction: the sub-micron particle regime for exponential and van der waals interactions. *Physics of Fluids* **25** (1), 012001.
- STONE, HOWARD A & SAMUEL, ARAVINTHAN DT 1996 Propulsion of microorganisms by surface distortions. *Physical review letters* **77** (19), 4102.
- WEISSTEIN, ERIC W 2002 Legendre polynomial. *Wolfram Research, Inc.* (<http://mathworld.wolfram.com/LegendrePolynomial.html>) .
- ZARE, YASSER, PARK, SANG PHIL & RHEE, KYONG YOP 2019 Analysis of complex viscosity and shear thinning behavior in poly (lactic acid)/poly (ethylene oxide)/carbon nanotubes biosensor based on carreau–yasuda model. *Results in Physics* **13**, 102245.